

## Halogenated Additive-Driven Morphology Optimization Enables Universal Performance Enhancement in Multiple Electron Acceptors-Based Organic Solar Cells

Yijie Nai, <sup>[a]</sup> Wei Liu, <sup>[a] [b]</sup> Jun Yuan, \*, <sup>[a]</sup> Weikun Chen, <sup>[a]</sup> Keming Li, <sup>[c]</sup> Yuan Gao, <sup>[d]</sup> Jie Min, <sup>[d]</sup> Yitong Ji, <sup>[e]</sup> Wenchao Huang, <sup>[e]</sup> Kaizhi Gu, <sup>[f]</sup> Haoqing Ning, <sup>[c]</sup> Tong Wang, \*, <sup>[c]</sup> Xueyi Guo, <sup>[b]</sup> and Yingping Zou \*, <sup>[a] [f]</sup>

<sup>[a]</sup>College of Chemistry and Chemical Engineering, Central South University, Changsha, 410083, P. R. China

<sup>[b]</sup>School of Metallurgy and Environment, Central South University, Changsha, 410083, P. R. China

<sup>[c]</sup>Department of Chemistry and Centre for Processable Electronics, Imperial College London, London W12 0BZ, United Kingdom

<sup>[d]</sup>The Institute for Advanced Studies, Wuhan University, Wuhan 430072, P. R. China

<sup>[e]</sup>School of Materials Science and Engineering, Wuhan University of Technology, Wuhan 430070, China

<sup>[f]</sup>Institute for Advanced Study, Central South University, Changsha, 410083 P. R. China

\*Corresponding authors

E-mail: junyuan@csu.edu.cn; t.wang19@imperial.ac.uk; yingpingzou@cus.edu.cn

### Contents

I. Experimental section .....	1
Materials .....	1
Synthesis Procedures .....	2
Instruments and Measurements.....	4
Device Fabrication and Characterization.....	6
II. <sup>1</sup> H NMR and <sup>13</sup> C NMR Spectra Results.....	7
III. Additional Figures.....	12
IV. Additional Tables.....	18

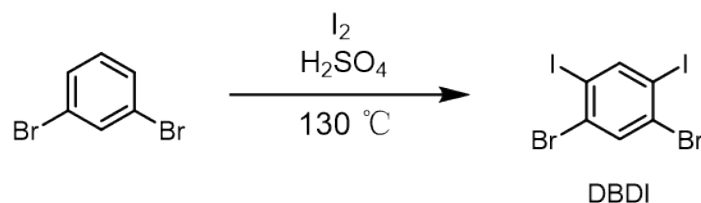
## I. Experimental section

### Materials

(1) Polymer donor PM6, (2,6-(4,8-bis(5-(2-ethylhexyl)-4-fluorothiophen-2-yl)-benzo[1,2-b:4,5b']-dithiophene)-co-(1,3-bis(thiophen-2-yl)-5,7-bis(2-ethylhexyl) benzo-[1,2-c:4,5-c']dithiophene-4,8-dione)), 1,4-dibromobenzene, 1,5-dibromo-2,4-difluorobenzene (DBDF), etc. were purchased from Solarmer, Inc (Beijing). Unless otherwise noted, all other chemicals were Energy Chemical, Derthon Optoelectronic Materials Co., Ltd., Yirou Photovoltaic Technology Co., Ltd, hwrk chem. Co Ltd or other commercial resources and used without further purification.

(2) All other reagents and solvents were purchased commercially as analytically pure and used without further purification; DFDB was purified before use.

(3) The main synthetic procedures of 1,5-dibromo-2,4-diiodobenzene (DBDI) is shown in **Fig. S1**:



**Figure S1.** Synthesis procedure for compound DBDI.

### Synthesis Procedures

**Synthesis of DBDI.** In a 500 mL three-neck round-bottom flask, 1,4-dibromobenzene (2.0 g, 8.5 mmol) was dissolved in 100 mL of concentrated sulfuric acid under heating. Elemental iodine (11.8 g, 46.6 mmol) was subsequently added, affording a deep purple solution, which was stirred at 130 °C for 48 hours. Upon cooling to room temperature, the reaction mixture was quenched with ice water and extracted with dichloromethane. The combined organic layers were washed with 200 mL of dilute sodium hydroxide solution to remove residual iodine, followed by successive washes with deionized water and brine. The organic phase was dried over anhydrous magnesium sulfate, filtered, and concentrated under reduced pressure. The resulting crude product was recrystallized from a dichloromethane/methanol mixed solvent system and further purified by column chromatography to afford the desired product as a white solid. (3.8 g, 92%). <sup>1</sup>H NMR (400 MHz, Chloroform-*d*) δ 8.28 (s, 1H), 7.84 (s, 1H).

**DBDF.** DBDF was purified through recrystallization. <sup>1</sup>H NMR (600 MHz, Chloroform-*d*) δ 8.28 (s, 1H), 7.84 (s, 1H).

## Instruments and Measurements

$^1\text{H}$  NMR spectra were recorded using a Bruker AV-600 spectrometer in a deuterated chloroform solution at 298 K, unless specified otherwise. Chemical shifts are reported as  $\delta$  values (ppm) with tetramethylsilane (TMS) as the internal reference. Thermogravimetric analysis (TGA) was conducted on a Perkin-Elmer TGA-7 with a heating rate of 10 K/min under nitrogen. UV-*Vis* absorption spectra were recorded on the SHIMADZU UV-2600 spectrophotometer. The cyclic voltammetry results were obtained with a computer-controlled CHI 660E electrochemical workstation.

The morphologies of the PM6:L8-BO blend films were investigated by atomic force microscopy (AFM, Agilent Technologies, 5500 AFM/SPM System, USA) in contacting mode with a  $5\mu\text{m}$  scanner. Transmission electron microscopy (TEM) measurement was performed in a JEM-2100F. Samples for TEM measurement were prepared as following: The active layer films were spin-cast on Glass/ITO/PEDOT:PSS substrates, and the substrates with active layers were submerged in deionized water to make the active layers float onto the air-water interface. Then, the floated films were picked upon unsupported 200 mesh copper grids for the TEM measurements.

The grazing-incidence wide-angle X-ray scattering (GIWAXS) measurement was carried out with a Xeuss 3.0 SAXS/WAXS laboratory beamline using a Cu X-ray source (8.05 keV, 1.54 Å) and a Pilatus 100K detector. The incident angle was  $0.18^\circ$  and the detector distance was 75mm. The samples for GIWAXS measurements were fabricated on silicon substrates using the same recipe for the devices.

Density Functional Theory (DFT) calculation. The ground-state geometries were optimized at PBE0/def2-SVPP level with Grimme's D3 dispersion correction with BJ dampening. The structural optimization of the dimerized solid additive and the complex of PM6-2mer/L8-BO with solid additive was carried out at same level. All the alkyl chains were replaced with methyl groups. The bonding energies ( $E_b$ ) were determined from the difference in total energies between the complexes

and their respective optimized interacting molecules.<sup>[1]</sup> All the calculations were performed with Gaussian 16 program (Rev C.01).

### **Device fabrication and characterization**

These devices are fabricated in conventional structure Glass/ITO/2-PACz/PM6:L8-BO/PNDIT-F3N/Ag. The substrates utilized were pre-patterned indium tin oxide (ITO) coated glasses with a sheet resistance of  $10 \Omega \text{ sq}^{-1}$ , which are cleaned through a series of steps including sequential sonicated in detergent-infused water, deionized water and isopropanol subsequently for 15min, and then blown dry with high purity nitrogen. The cleaned ITO glasses were treated with ultraviolet ozone cleaning system for 25 min firstly, then transferred into the nitrogen-filled glove box. subsequently spin-coated the 2-PACz solution onto it at a speed of 3000rpm for 30s and annealed at 100°C for 10 min. A blend of PM6 donor and L8-BO acceptor was dissolved in chloroform (CF) with a total concentration of 16.1 mg/mL for 2 h and spin-coat at 3600 rpm for 30 s onto the 2-PACz layer. For the SAs-processed devices, SAs were first dissolved in CF at 10 mg/ml for about 30 min, and then PM6:L8-BO blend was dissolved in the solution configured with SAs at a total weight concentration of 16.1 mg/ml. The thermal annealing treatment of the active layer was performed at 100°C for 10 min. After cooling to room temperature, PNDIT-F3N dissolved in methanol at a concentration of 1 mg/mL with 0.5 wt.% acetic acid was spin-deposited onto the active layers at a speed of 3000 rpm for 30 s. Finally, the metal cathode Ag was thermally evaporated through a mask onto the cathode buffer layer with a base pressure of approximately  $1.5 \times 10^{-4} \text{ Pa}$ . The photovoltaic area of the device is  $0.0484 \text{ cm}^2$ . The tests of the device's photoelectric properties were conducted in nitrogen-filled glove box, and all the devices used were not encapsulated.

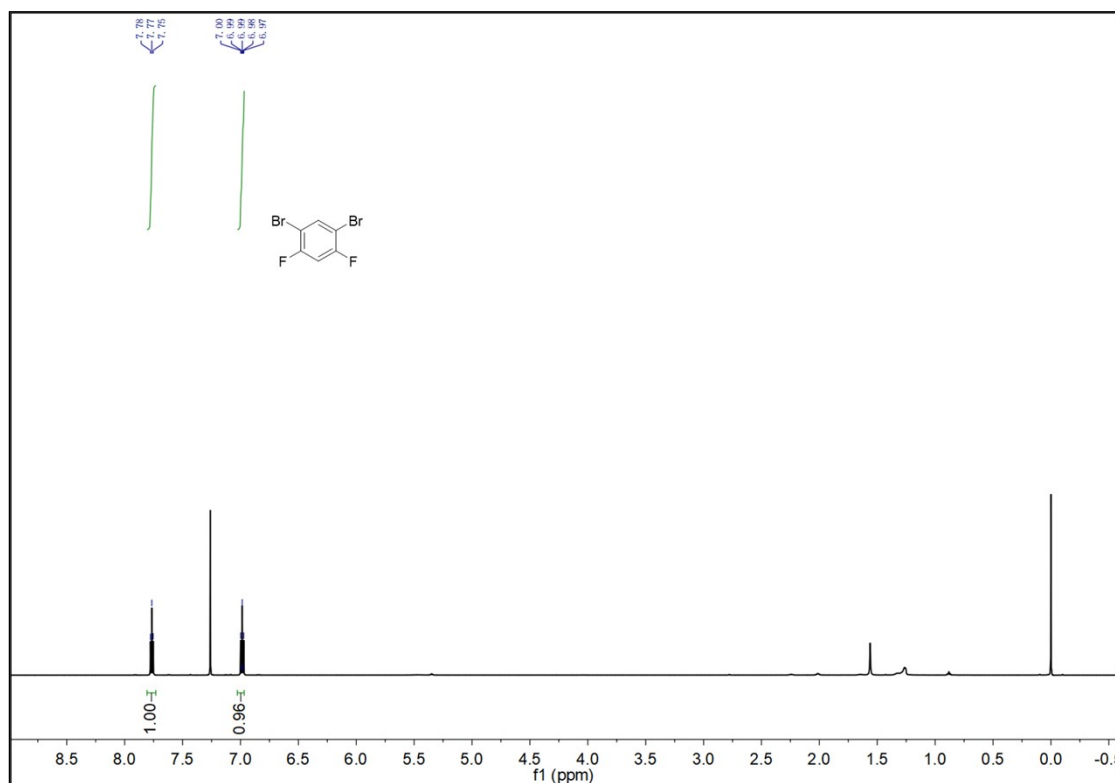
The current density-voltage ( $J$ - $V$ ) characteristics of the devices were measured under simulated AM1.5G irradiation ( $100 \text{ mW/cm}^2$ ) using an SS-F5-3A solar simulator (Enli Technology, Inc.) equipped with a Xe lamp. Prior to the performance measurement, light intensity was calibrated using a silicon photodiode with a KG5 filter certified by the National Renewable Energy Laboratory. The EQE spectra measurement were performed on a commercial EQE measurement system (QE-R, Enli Technology, Inc.). Light intensity dependent  $V_{\text{OC}}$  and  $J_{\text{SC}}$  measurement were performed on a  $J$ - $V$  measurement system with light intensities ranging from 0.1 sun to 1 sun.

Electron mobility and hole mobility measurements. The charge carrier mobilities were measurement with the device structure of Glass/ITO/PEDOT:PSS/active layer/MoO<sub>3</sub>/Ag for hole mobility and Glass/ITO/ZnO/active layer/PNDIT-F3N/Ag for electron mobility. The hole and electron mobilities were calculated according to the space charge limited current (SCLC) MOTT-Gurney equation:

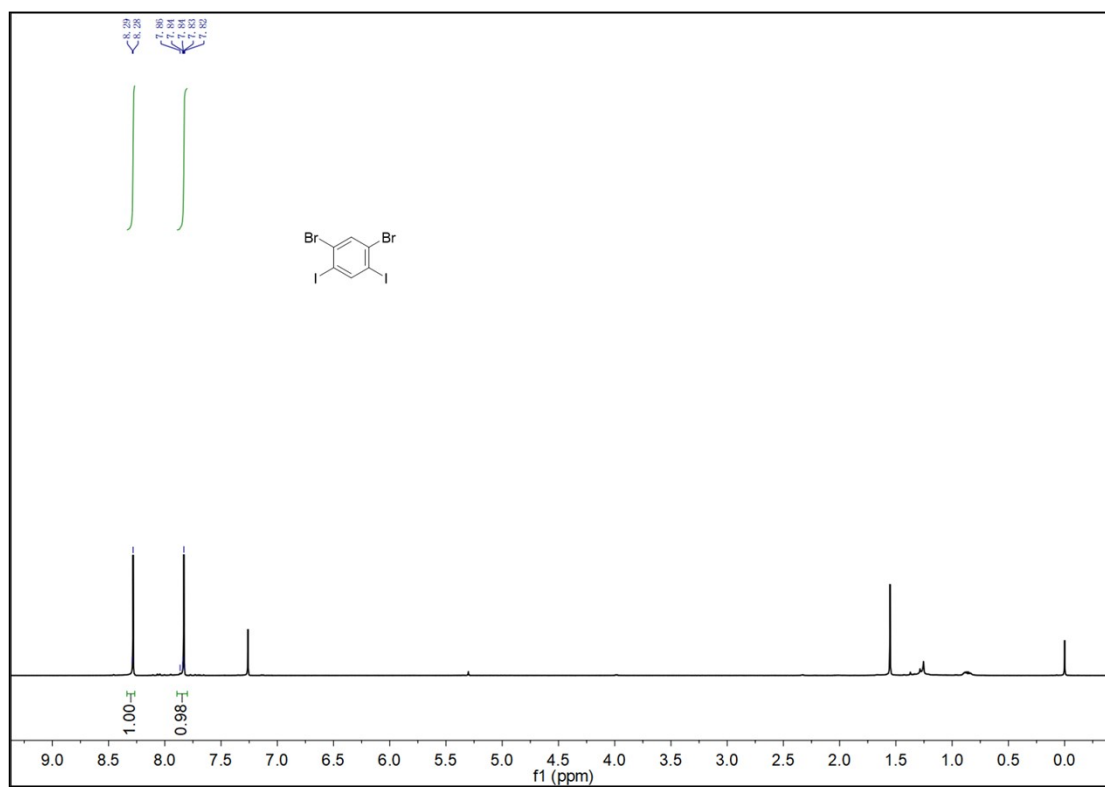
$$J = \frac{9\varepsilon_0\varepsilon_r\mu V^2}{8d_3}$$

Where  $J$  is the current density,  $\mu$  is the zero-field mobility,  $\varepsilon_0$  is the permittivity of free space,  $\varepsilon_r$  is the relative permittivity of the material, typically ranging from 2-4 for organic/polymer semiconductors, and in this case, a dielectric permittivity of 3 was implemented for polymer.  $d$  is the thickness of the active layers, and  $V$  is the internal voltage within the device. The internal voltage was obtained by subtracting the built-in voltage ( $V_{bi}$ ) from the series resistance of the whole device except for the active layers from the applied voltage ( $V_{appl}$ ),  $V = V_{appl} - V_{bi}$  (in the hole-only and electron-only devices, the  $V_{bi}$  values can be disregarded). The mobility can be calculated from the slope of the  $J^{1/2}$ - $V$  curves.

## II. <sup>1</sup>H NMR Spectra Results

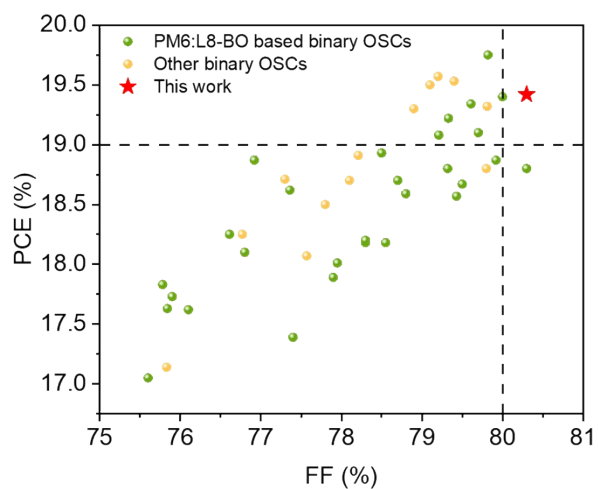


**Figure S2.**  $^1\text{H}$  NMR spectrum of compound DBDF in  $\text{CDCl}_3$ .

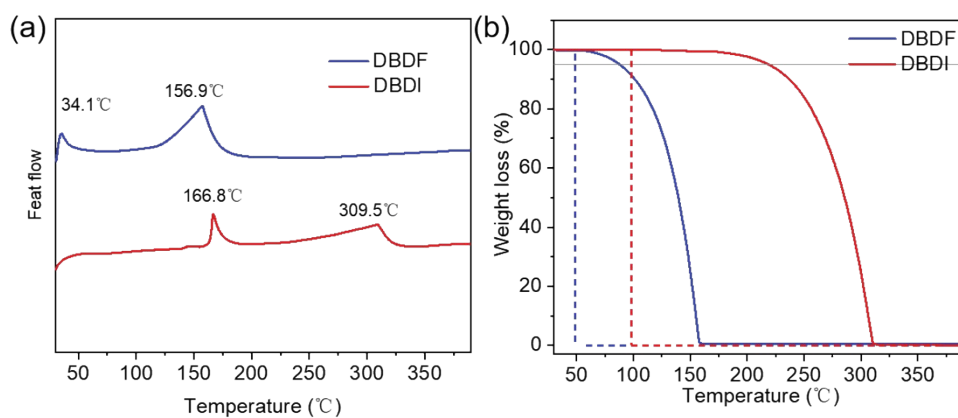


**Figure S3.**  $^1\text{H}$  NMR spectrum of DBDI in  $\text{CDCl}_3$ .

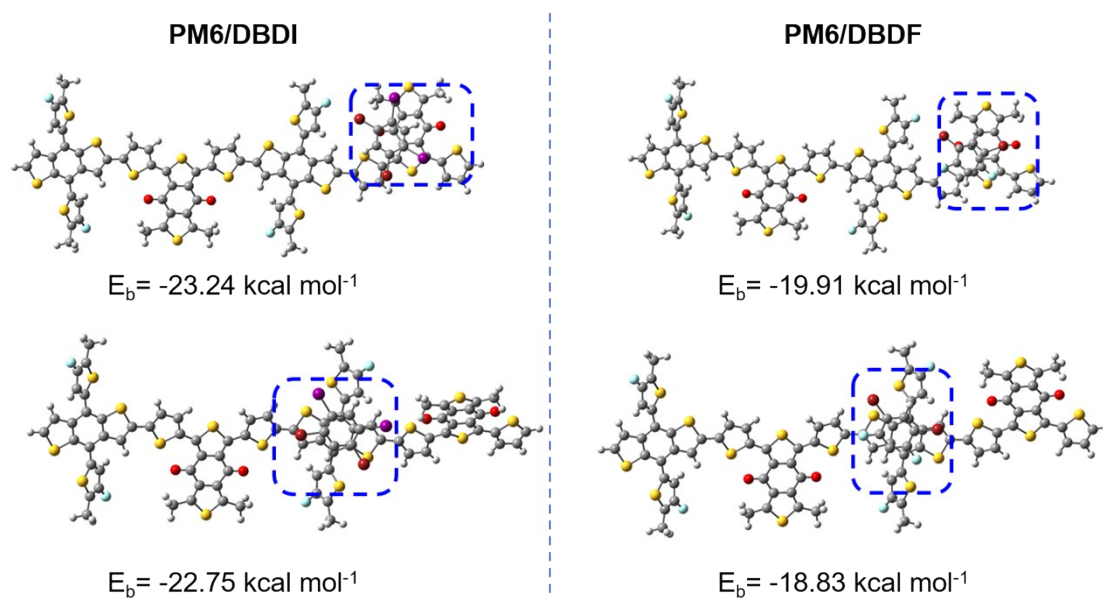
### III. Additional Figures



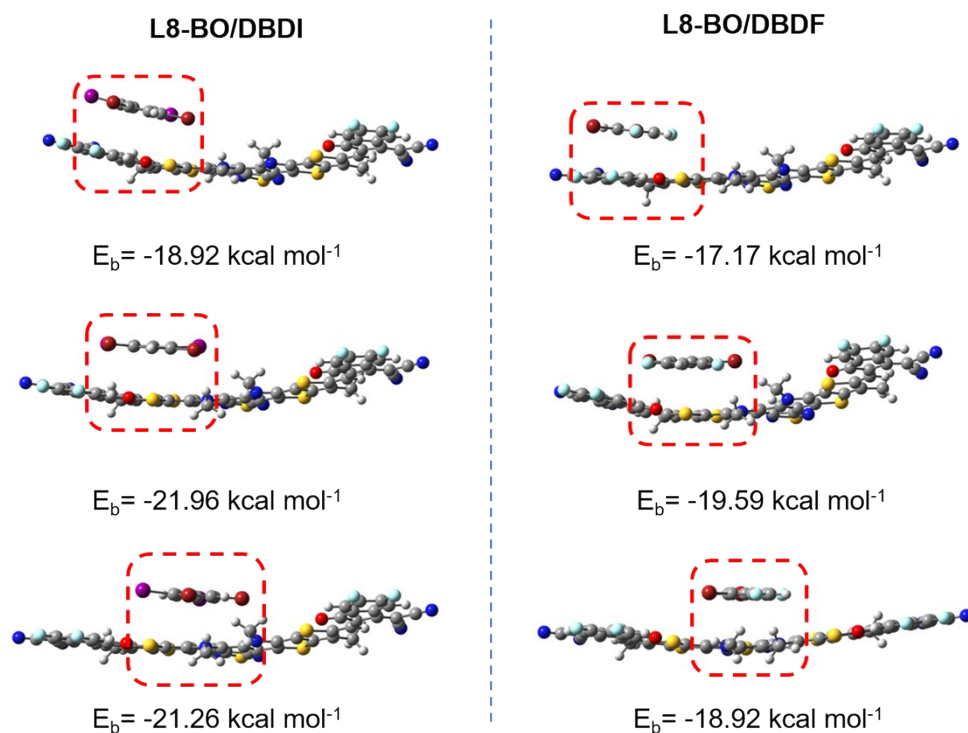
**Figure S4.** Summary of additives used in PM6:L8-BO and other system-based binary OSCs.



**Figure S5.** The (a) DSC and (b) TGA curves of DBDF and DBDI.

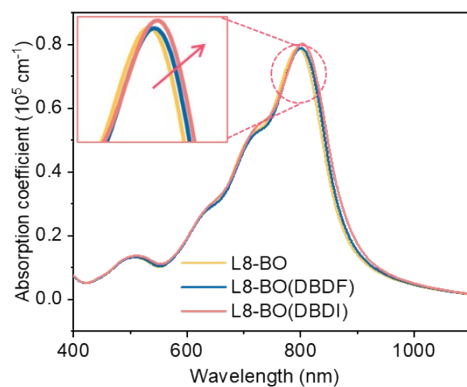


**Figure S6.** The optimized geometry model of complexes of PM6 with DBDF (PM6/DBDF complexes) and complexes of PM6 with DBDI (PM6/DBDI) complexes.

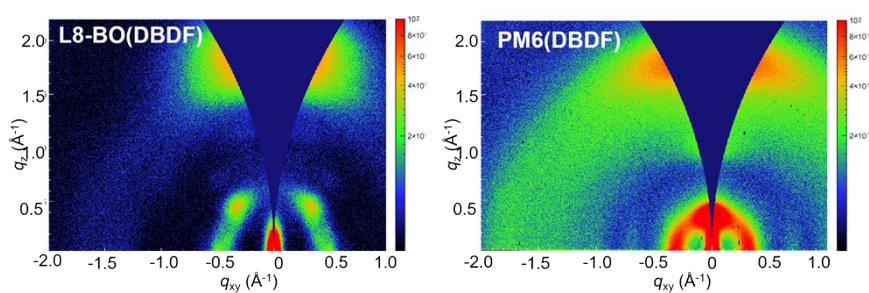


**Figure S7.** The optimized geometry model of complexes of L8-BO with DBDF (L8-BO/DBDF complexes) and complexes of L8-BO with DBDI (L8-BO/DBDI) complexes.

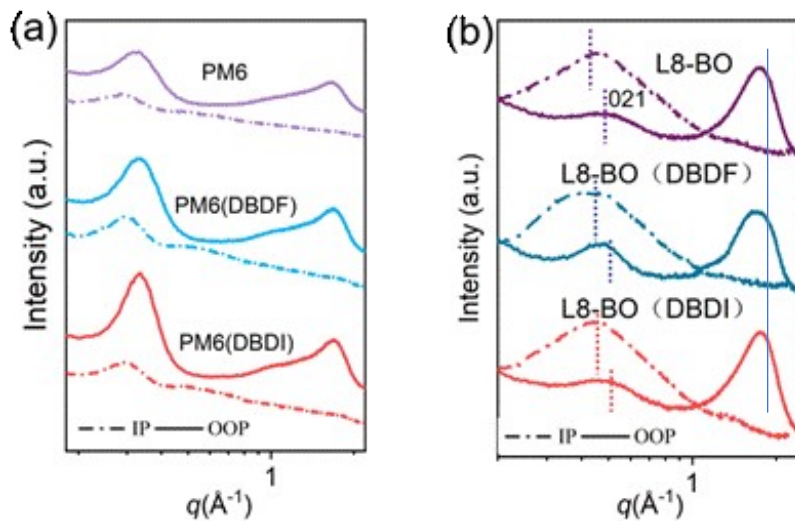




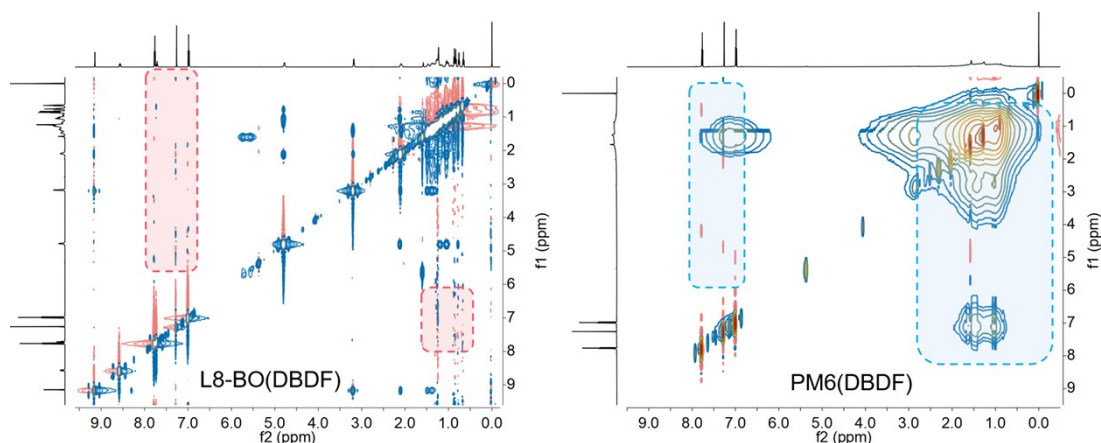
**Figure S8.** L8-BO, L8-BO(DBDF) and L8-BO (DBDI) films with TA process.



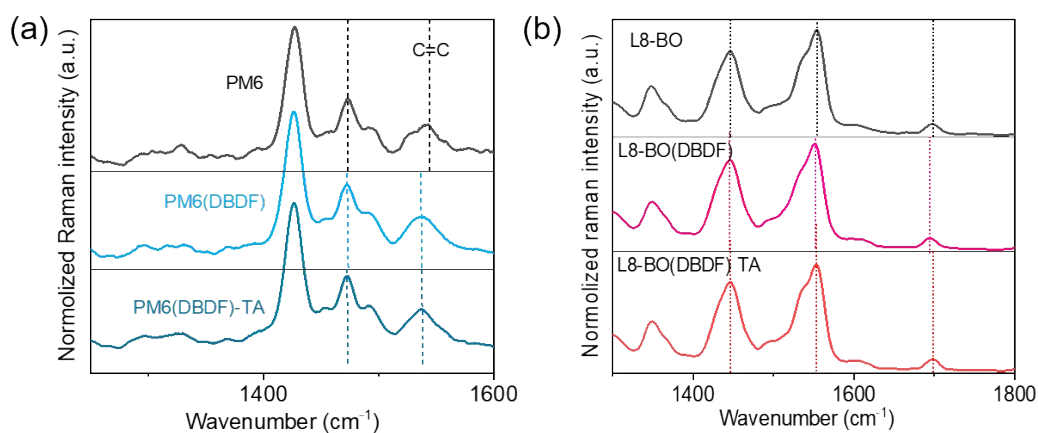
**Figure S9.** 2D GIWAXS patterns of the L8-BO treated with DBDF, and PM6 treated with DBDF films.



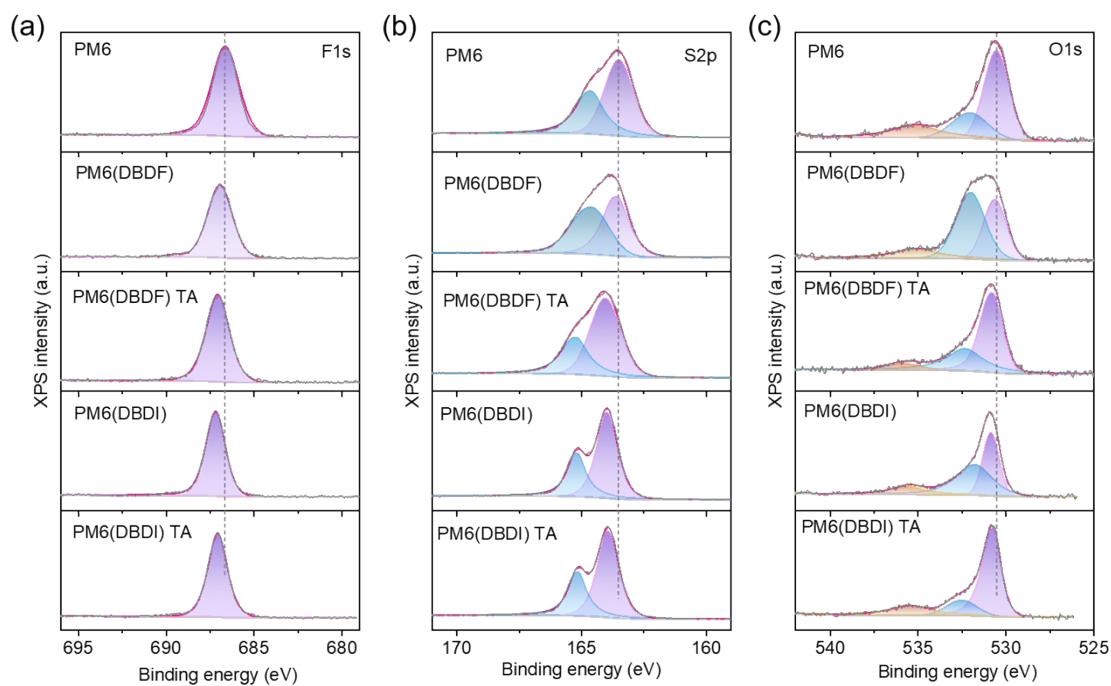
**Figure S10.** GIWAXS 1D profiles of (a) PM6 and (b) L8-BO treated with W/O and DBDF films.



**Figure S11.** 2D  $^1\text{H}$ - $^1\text{H}$  NMR spectra of L8-BO(DBDF) and PM6(DBDF).

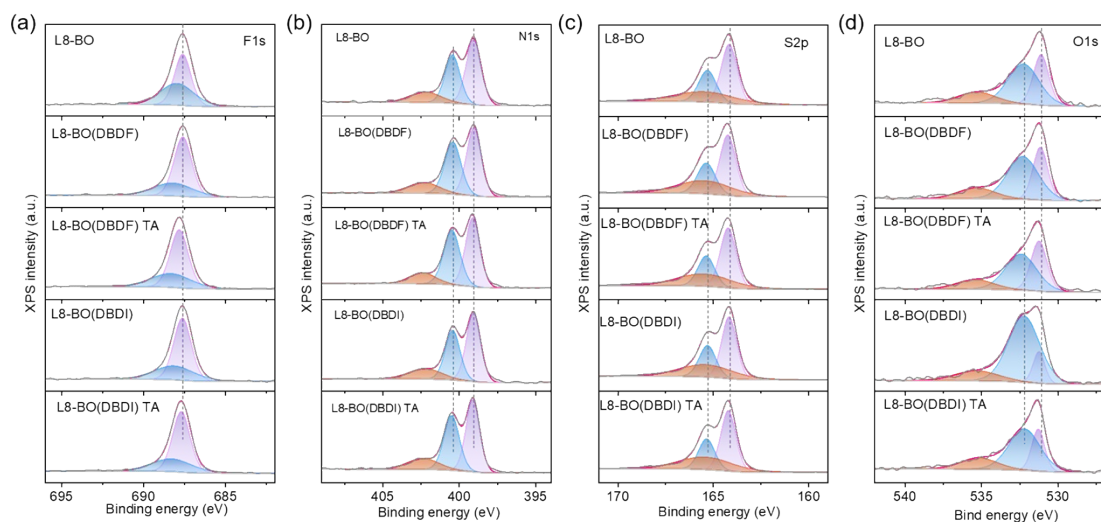


**Figure S12.** Raman spectra of (a) PM6 and (b) L8-BO treated with W/O and DBDF films.

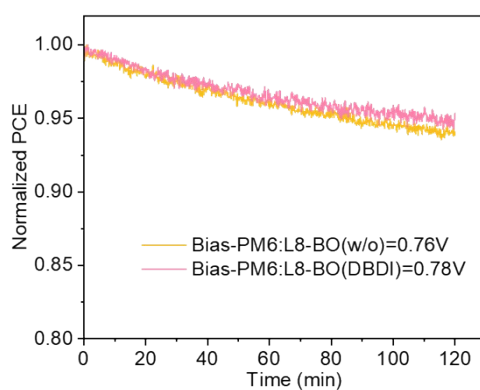


**Figure S13.** F(1s), S (2p) and O(1s) XPS spectra of PM6, PM6(DBDF) and PM6(DBDI) systems

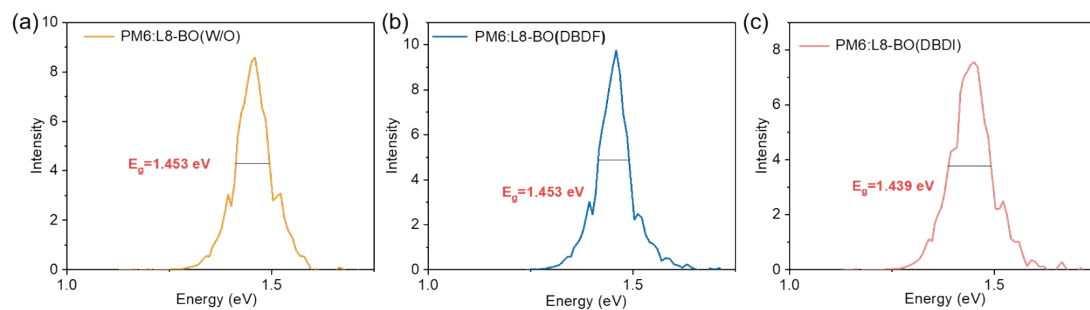
before and after TA.



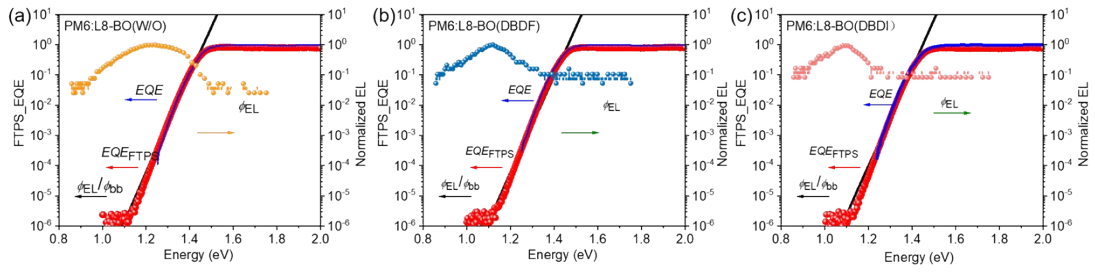
**Figure S14.** F(1s), S (2p), N(1s) and O(1s) XPS spectra of L8-BO, L8-BO(DBDF) and L8-BO(DBDI) systems before and after TA.



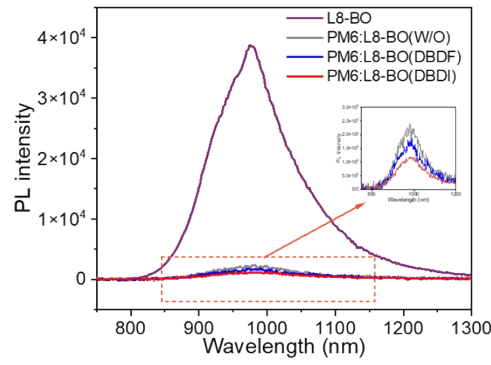
**Figure S15.** Operational stability comparison between devices based on PM6:L8-BO(DBDI) and PM6:L8-BO(w/o) system under the maximum power point tracking.



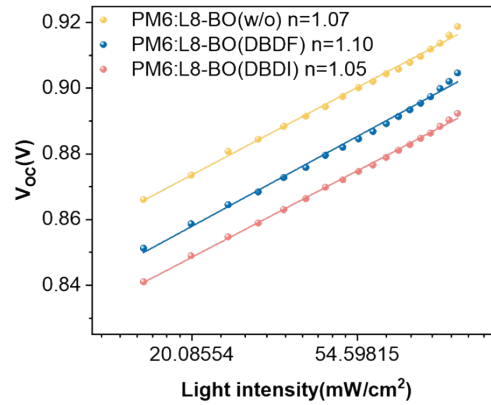
**Figure S16.**  $E_g$  of the (a) PM6:L8-BO(w/o), (b) PM6:L8-BO(DBDF) and (c) PM6:L8-BO(DBDI) calculated from the precise measurement of their corresponding EQE.



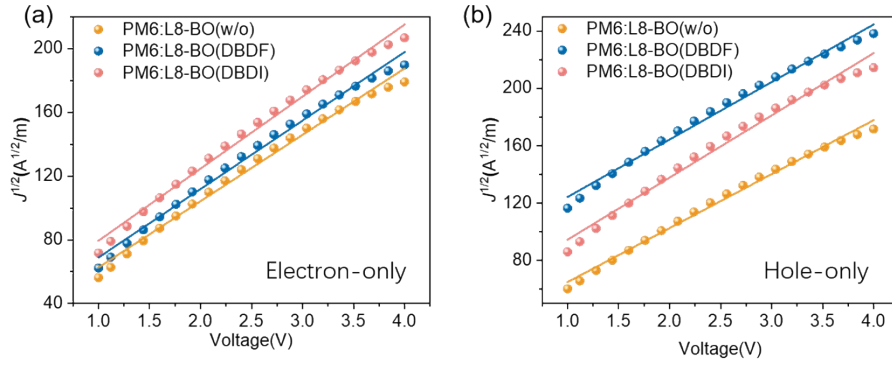
**Figure S17.** Semi-logarithmic plots of normalized EL, measured EQE and EQE calculated by FTPS (EQEFTPS) as a function of energy for devices based on (a) PM6:L8-BO(w/o), (b) PM6:L8-BO(DBDF) and (c) PM6:L8-BO(DBDI).



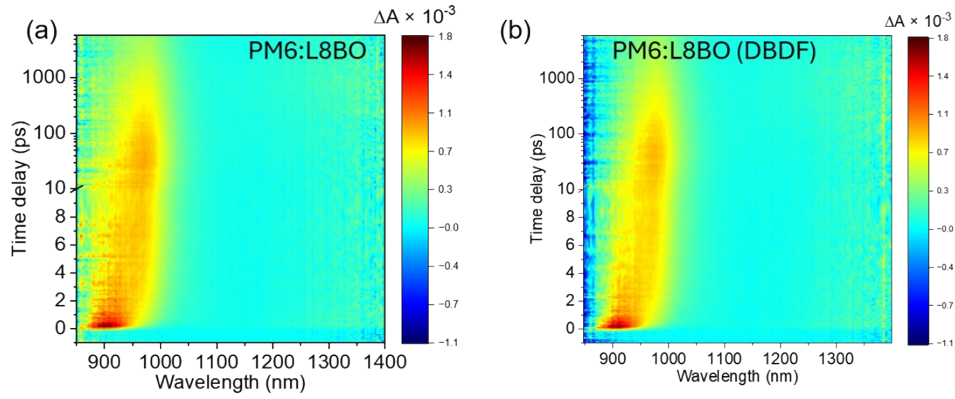
**Figure S18.** PL spectrum of L8-BO, PM6:L8-BO, PM6:L8-BO(DBDF) and PM6:L8-BO(DBDI) films.



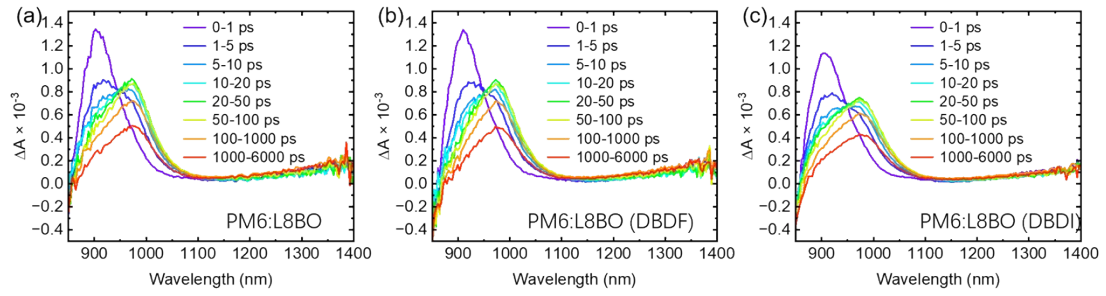
**Figure S19.** The curves of  $V_{OC}$  vs  $\ln P$  for the OSCs based on PM6:L8-BO without/with different additives.



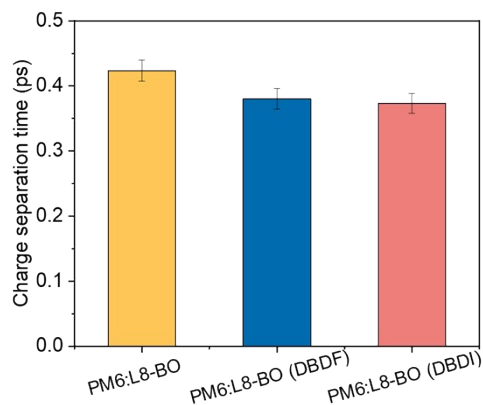
**Figure S20.** The dark  $J^{1/2}$ - $V$  curves of electron-only (a) and hole-only (b) PM6:L8-BO devices without additives or with DBDF and DBDI additives.



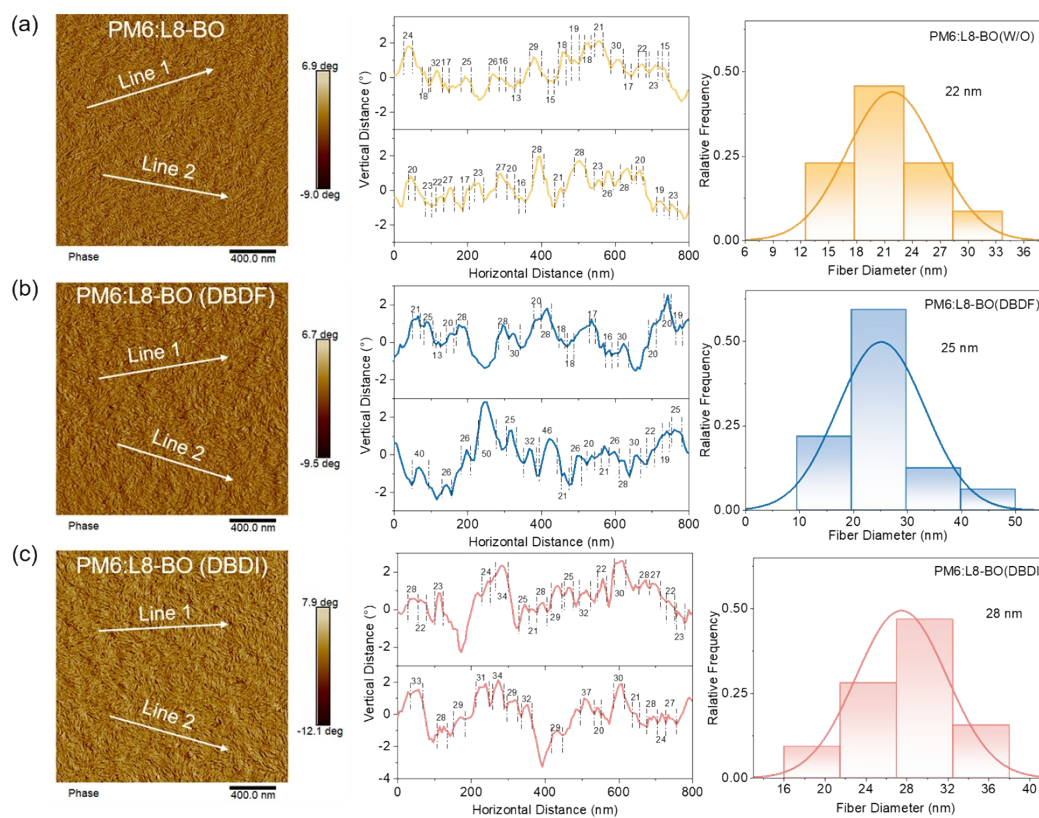
**Figure S21.** Femtosecond transient absorption spectra of the blend films of (a) PM6:L8-BO and (b) PM6:L8-BO(DBDF)



**Figure S22.** The TA spectra of blend films of a) PM6:L8-BO(W/O), b) M6:L8-BO(DBDF) and c) M6:L8-BO(DBDI) recorded at varied probe delay times.

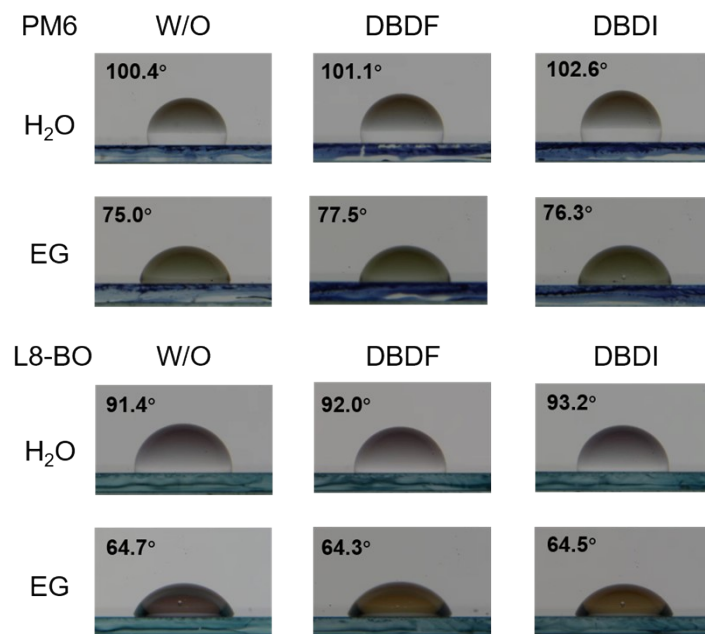


**Figure S23** The average charge separation times of PM6:L8-BO, PM6:L8-BO(DBDF) and PM6:L8-BO(DBDI) system.

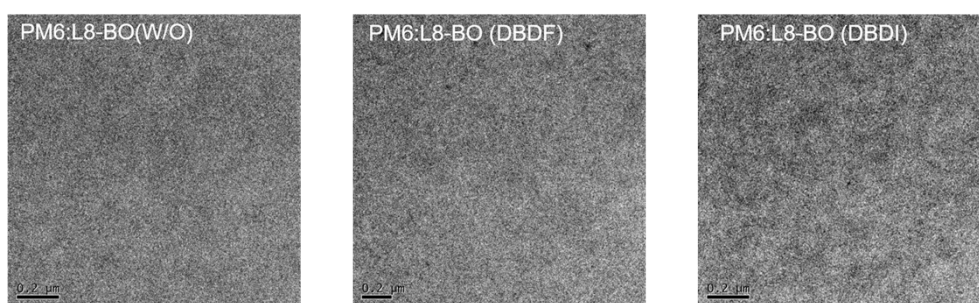


**Figure S24.** The AFM phase images of blend films and the corresponding fiber diameter summary of (a) PM6:L8-BO, (b) PM6:L8-BO(DBDF) and (c) PM6:L8-BO(DBDI).

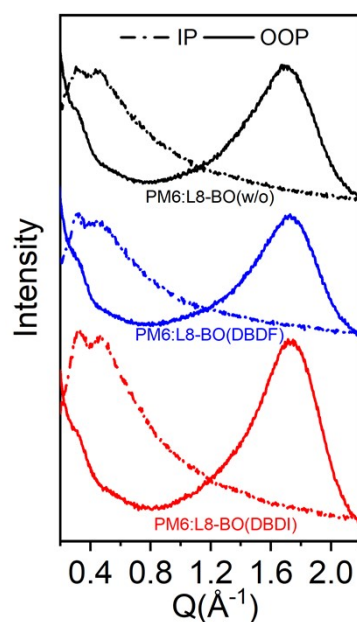




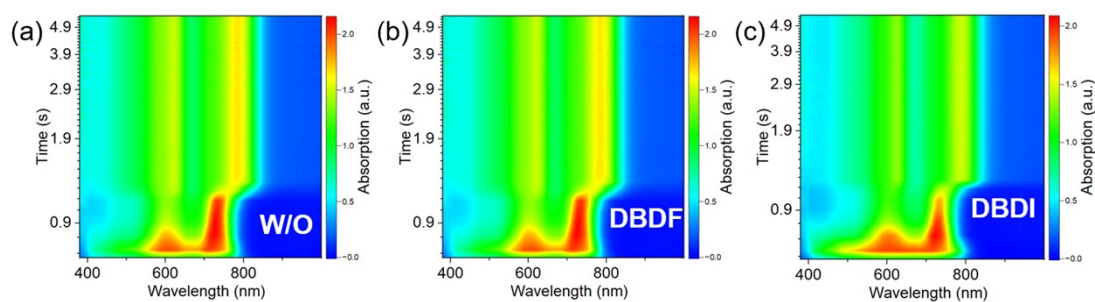
**Figure S25.** Contact angle images of various films with diverse additives.



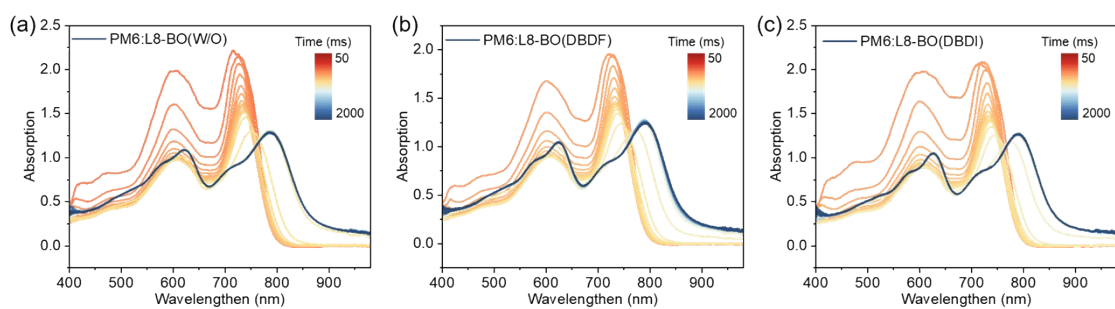
**Figure S26.** The TEM images of blend films of PM6:L8-BO, PM6:L8-BO(DBDF) and PM6:L8-BO(DBDI).



**Figure S27.** GIWAXS 1D profiles of PM6:L8-BO treated with W/O, DBDF and DBDI films.

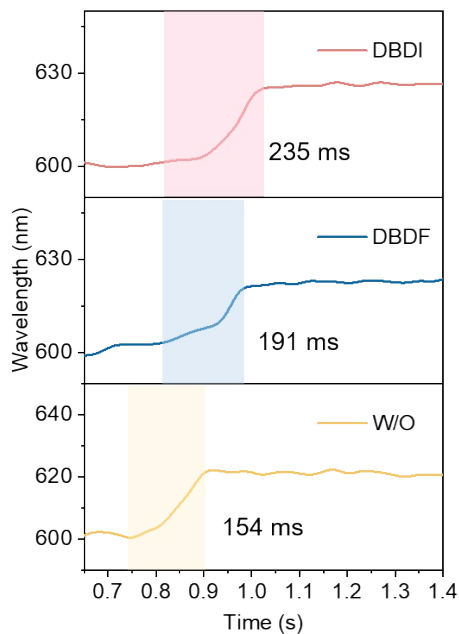


**Figure S28.** Time evolution of UV-vis absorption contour maps.

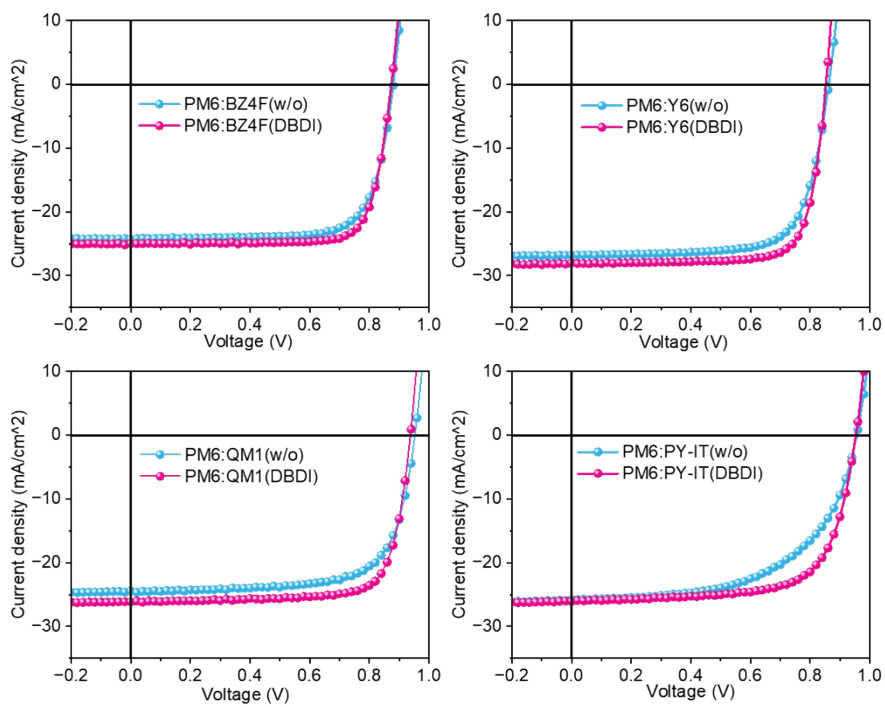


**Figure S29.** The captured UV-vis spectra a) in PM6:L8-BO(W/O), b) PM6:L8-BO with DBDF and c) PM6:L8-BO with DBDI additive during CF drop casting.

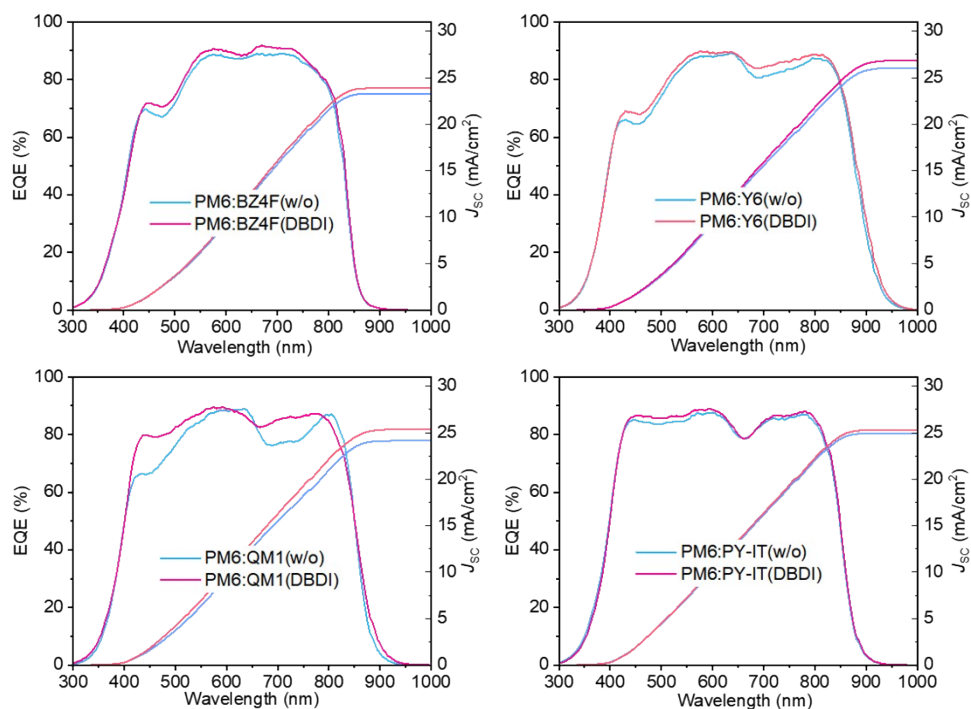




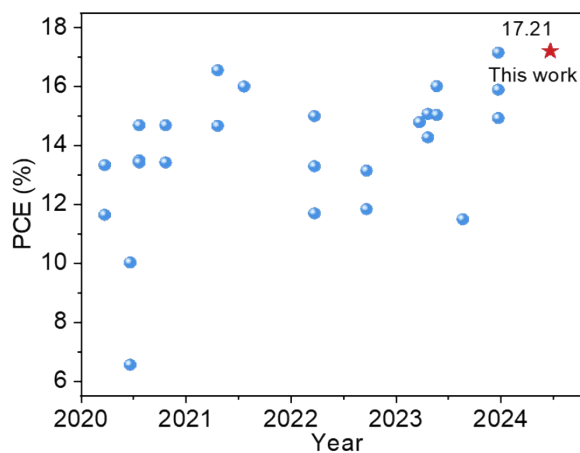
**Figure S30.** The time evolution of PM6 peak position and intensity in blend films.



**Figure S31.** (a)  $J$ - $V$  curves of PM6:Y6, PM6:PY-IT and PM6:BZ4F TA blend films treated without and with DBDI.




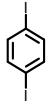
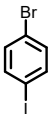
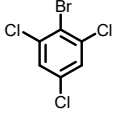
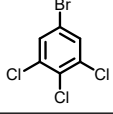
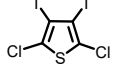
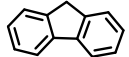
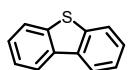
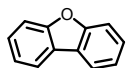
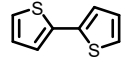
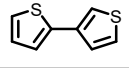
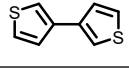
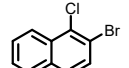
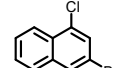
**Figure S32.** EQE curves of PM6:Y6, PM6:PY-IT and PM6:BZ4F TA blend films treated without and with DBDI.

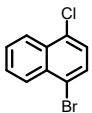
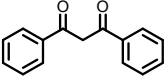
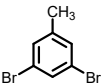
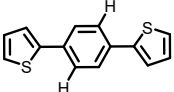
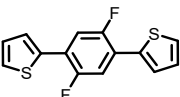
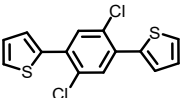
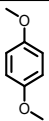
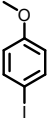

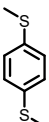
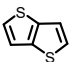
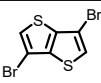
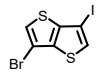


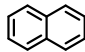
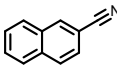
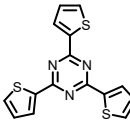
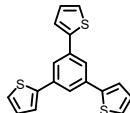
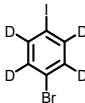
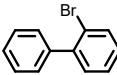
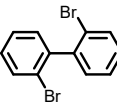
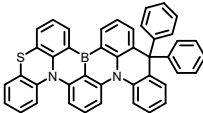
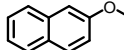
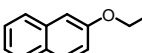
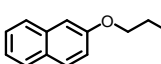
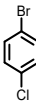
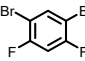
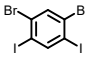
**Figure S33.** Plots of PCE versus Year, based on the reported A-DA'D-A-type pentacyclic fused-ring SMAs binary OSCs in recent five years.

#### IV. Additional Tables

**Table S1.** Summary of PM6-series based binary OSCs with solid additives treatment.

Active layer	additive	Structure	VOC (V)	JSC (mA/cm <sup>2</sup> )	FF (%)	PCE (%)	
PM6:BTP-cC9	w/o		0.861	25.86	73.87	16.44	[2]
	DBB		0.862	26.22	75.83	17.14	
	DIB		0.860	27.58	76.77	18.25	
	BIB		0.867	27.89	78.21	18.91	
PM6:L8-BO	w/o		0.901	25.02	71.37	16.09	[3]
	TCBB-1		0.892	27.03	78.50	18.93	
	TCBB-2		0.882	26.20	77.95	18.01	
PM6:L8-BO	w/o		0.908	25.22	73.9	16.9	[4]
	SA-T5		0.879	26.65	80.3	18.8	
PM6:L8-BO	w/o		0.902	25.61	71.70	16.60	[5]
	FL		0.885	26.64	76.80	18.10	
	DBT		0.877	26.52	75.84	17.63	
	DBF		0.893	27.01	77.36	18.62	
PM6:L8-BO	w/o		0.937	25.09	71.83	16.89	[6]
	2,2-TT		0.895	26.49	79.32	18.80	
	2,3-TT		0.913	26.54	79.33	19.22	
	3,3-TT		0.916	26.52	79.61	19.34	
PM6:L8-BO	w/o		0.893	25.89	74.3	17.17	[7]
	<i>o</i> -BrCN		0.879	26.12	77.9	17.89	
	<i>m</i> -BrCN		0.879	25.55	77.4	17.39	

	<i>p</i> -BrCN		0.881	26.35	78.3	18.18	
PM6:Y6	DBM+TA		0.830	28.7	78.1	18.7	[8]
PM6:BTP-cC9	w/o		0.855	26.7	74.1	16.9	
	DBM+TA		0.844	28.2	77.8	18.5	
PM6:L8-BO	w/o		0.905	25.55	71.92	16.63	[9]
	DTL		0.906	27.06	76.92	18.87	
PM6:L8-BO	w/o		0.907	25.79	74.3	17.37	[10]
	D1-H		0.867	26.71	76.1	17.62	
	D1-F		0.873	26.76	75.9	17.73	
	D1-Cl		0.886	26.62	78.8	18.59	
PM6:L8-BO	w/o		0.907	24.77	73.36	16.49	[11]
	DOB		0.900	25.05	75.60	17.05	
	OIB		0.910	25.86	75.78	17.83	
	DIB		0.893	26.17	79.43	18.57	
	SIB		0.898	26.30	79.92	18.87	
PM6:L8-BO	w/o		0.895	25.0	75.6	16.9	[12]
	TT		0.886	26.3	78.3	18.2	
	TTBB		0.893	26.8	79.7	19.1	
	TTBI		0.889	26.7	78.7	18.7	
	TTBB/TTBI		0.898	26.9	80.0	19.4	
PM6:L8-BO	w/o		0.908	26.06	74.54	17.43	[13]

	NA		0.886	26.12	78.55	18.18	
	2-CAN		0.892	27.00	79.21	19.08	
PM6:L8-BO	w/o		0.909	25.92	75.09	17.69	[14]
	T3T		0.907	26.25	76.61	18.25	
	B3T		0.891	27.78	79.82	19.75	
PM6:L8-BO	w/o		0.900	24.59	74.60	16.51	[15]
	p-IBrPh-d4		0.885	26.53	79.50	18.67	
PM6:BTP-eC9	w/o		0.857	27.77	76.11	18.12	
	p-IBrPh-d4		0.856	28.27	79.81	19.32	
PM6:BTP-eC9	w/o		0.871	26.57	73.70	17.06	[16]
	BB		0.855	27.23	77.57	18.07	
	DBB		0.860	28.78	79.20	19.57	
PM6:BTP-eC9	w/o		0.849	26.7	77.8	17.6	[17]
	BNS-H1		0.848	27.7	79.8	18.8	
PM6:PY-T-X	w/o		0.958	24.83	65.6	15.60	[18]
	2-MN		0.951	25.45	77.3	18.71	
	2-EN		0.953	25.87	79.1	19.5	
	2-PN		0.952	25.70	78.9	19.30	
PM6:BTP-eC9	w/o		0.858	27.39	73.9	17.36	[19]
	BCB		0.864	28.47	79.4	19.53	
PM6:L8-BO	w/o		0.915	25.63	73.9	17.37	This work
	DBDF		0.910	25.72	78.2	18.34	
	DBDI		0.905	26.80	80.3	19.42	

**Table S2.** GIWAXS data of the neat L8-BO films.

OOP plane					
Films	diffraction	Q (Å <sup>-1</sup> )	D-spacing (Å)	FWHM (Å <sup>-1</sup> )	CCLs (Å)
L8-BO	(100)	0.467	13.45	0.214	26.42
	(010)	1.727	3.64	0.489	11.56
L8-BO(DBDF)	(100)	0.470	13.37	0.143	39.54
	(010)	1.718	3.64	0.560	10.10
L8-BO(DBDI)	(100)	0.480	13.09	0.180	31.41
	(010)	1.757	3.57	0.446	12.67
In plane					
Films	diffraction	Q (Å <sup>-1</sup> )	D-spacing (Å)	FWHM (Å <sup>-1</sup> )	CCLs (Å)
L8-BO	(021)	0.438	14.35	0.287	19.70
L8-BO(DBDF)	(021)	0.450	13.96	0.307	18.41
L8-BO(DBDI)	(021)	0.461	13.63	0.278	20.34

**Table S3.** GIWAXS data of the neat PM6 films.

OOP plane					
Films	diffraction	Q (Å <sup>-1</sup> )	D-spacing (Å)	FWHM (Å <sup>-1</sup> )	CCLs
PM6	(100)	0.321	19.57	0.118	47.92
	(010)	1.639	3.83	0.498	11.35
PM6(DBDF)	(100)	0.330	19.04	0.090	62.83
	(010)	1.667	3.77	0.444	12.74
PM6(DBDI)	(100)	0.337	18.64	0.085	66.52
	(010)	1.701	3.69	0.424	13.34
In plane					
Films	diffraction	Q (Å <sup>-1</sup> )	D-spacing (Å)	FWHM (Å <sup>-1</sup> )	CCLs (Å)
PM6	(100)	0.280	22.43	0.107	52.85
PM6(DBDF)	(100)	0.290	21.67	0.084	67.32
PM6(DBDI)	(100)	0.302	20.80	0.080	70.68

**Table S4.** Energy loss profile of the PM6:L8-BO(w/o), (b) PM6:L8-BO(DBDF) and (c)

PM6:L8-BO(DBDI)-based OSCs.

Active layers	$E_{gap}$ [eV]	$V_{oc}$ [V]	$V_{oc\ loss}$ [eV]	$V_{oc}^{SQ}$ [V]	$\Delta E_1$ [eV]	$V_{oc}^{rad}$ [V]	$\Delta E_2$ [eV]	$\Delta E_3$ [eV]
PM6:L8-BO (w/o)	1.453	0.915	0.538	1.195	0.258	1.102	0.093	0.187
PM6:L8-BO (DBDF)	1.453	0.910	0.543	1.195	0.258	1.104	0.091	0.194
PM6:L8-BO (DBDI)	1.439	0.905	0.534	1.181	0.258	1.089	0.092	0.184

**Table S5.** Gaussian-convoluted biexponential rise function fitting and calculating parameters for the TA decay curve.

	A1	t1 (ps)	A2	t2 (ps)	t ave (ps)
PM6:L8BO	0.66±0.01	0.30±0.02	0.31±0.01	5.03±0.41	0.42±0.02
PM6:L8BO(DBDF)	0.70±0.01	0.28±0.02	0.26±0.01	5.10±0.50	0.38±0.02
PM6:L8BO(DBDI)	0.72±0.01	0.28±0.01	0.25±0.01	6.96±0.48	0.37±0.02

**Table S6.** Parameters of contact angles and surface energies of films.

Samples	Contact		Surface Energy [mJ m <sup>-2</sup> ]	Relative $\chi^a$ (K)
	Water	Ethylene glycol		
PM6	100.4	75.0	22.40	0.053
L8-BO	91.4	64.7	24.63	
PM6(DBDF)	101.1	77.5	22.66	
L8-BO(DBDF)	92.0	64.3	26.15	0.125
PM6(DBDI)	102.6	76.3	23.58	
L8-BO(DBDI)	93.1	64.5	27.60	

**Table S7.** GIWAXS data of the blend films.

OOP plane					
Films	diffraction	Q (Å <sup>-1</sup> )	D-spacing (Å)	FWHM (Å <sup>-1</sup> )	CCLs (Å)
PM6:L8-	(100)	0.296	21.22	0.078	72.50

BO	(010)	1.679	3.74	0.465	12.16		
PM6:L8-BO(DBDF)	(100)	0.318	19.76	0.074	76.59		
	(010)	1.730	3.63	0.439	12.88		
PM6:L8-BO(DBDI)	(100)	0.322	19.46	0.072	78.30		
	(010)	1.746	3.60	0.431	13.12		
<b>In plane</b>							
Films	diffraction	Q (Å <sup>-1</sup> )	D-spacing (Å)	CCLs (Å)	diffraction	Q (Å <sup>-1</sup> )	D-spacing (Å)
PM6:L8-BO	(100)	0.302	20.80	46.67	(021)	0.439	14.31
PM6:L8-BO(DBDF)	(100)	0.319	19.69	54.76	(021)	0.449	13.99
PM6:L8-BO(DBDI)	(100)	0.330	19.04	67.88	(021)	0.468	14.42

- a. Crystalline coherence length (CCL) was calculated according to the Scherrer equation  $CCL = 2\pi K / \text{FWHM}$ , where K is the shape factor ( $K \approx 0.9$ ).<sup>[20]</sup>



**Table S8** The photovoltaic parameters of binary OSCs based on A-DA'D-A type pentacyclic acceptors.

Donor: acceptor	$V_{oc}$ (V)	$J_{sc}$ (mA/cm <sup>2</sup> )	FF	PCE	Ref.
PBCT-2F : BTPT4F-EH	0.92	18.8	0.677	11.7	[21]
PBCT-2F : BTPT4F-BO	0.89	22.0	0.763	15.0	[21]
PBCT-2F : BTPT4F-DH	0.89	19.9	75.1	13.3	[21]
PM6:BZ4F-O-1	0.91	19.57	75.61	13.50	[22]
PM6:BZ4F-O-2	0.82	21.62	74.74	13.43	[22]
PM6:BZ4F-O-3	0.85	23.51	73.72	14.69	[22]
PTQ10:Y26	0.886	23.57	76.73	16.01	[23]
PM6:BZ4F-EH	0.880	22.34	75.1	14.67	[24]
PM6:BZ4F-OEH	0.855	24.43	79.3	16.56	[24]
PM6: BZ4F-ch1	0.863	23.09	80.41	16.02	[25]
PM6: BZ4F-ch2	0.878	22.01	77.85	15.04	[25]
PTQ10:BZ4F-2C <sub>2</sub> SEH	0.845	23.45	75	14.80	[26]
PTQ10:BZ4F-C <sub>2</sub> SEH	0.870	23.27	75	15.08	[26]
PTQ10:BZ4F-SEH	0.886	21.99	73	14.28	[26]
PM6:L1-EH	0.809	20.03	73.0	11.84	[27]
PM6:L1-BO	0.848	20.76	74.4	13.15	[27]
PM6:BTT-4F	0.88	17.08	66.68	10.03	[28]
PM6:BTTCN-Cl	0.90	13.15	55.46	6.56	[28]
PBDCT:BT-F	0.914	22.09	73.97	14.93	[29]
PBDCT:BTA-C4-F	0.907	23.50	74.51	15.90	[29]
PBDCT:BTA-C4-Cl	0.894	25.52	75.26	17.16	[29]
PM6:BTP-C3	0.990	17.6	66.1	11.5	[30]
PM6:Y25	0.80	20.19	72.14	11.65	[31]
PM6:Y26	0.83	21.63	74.33	13.34	[31]
PM6:BZ4F	0.874	24.97	78.89	17.21	This work

## Reference

- [1] H. L. Zheng, Y. Q. Sang, K. N. Houk, X. S. Xue, J. P. Cheng, *J. Am. Chem. Soc.* **2019**, *141*, 16046-16056.
- [2] Z. Mei, R. Li, K. Li, Y. Wu, Y. Chen, H. Geng, Q. Liao, C. An, H. Fu, *Journal of Materials Chemistry A* **2024**, *12*, 28254-28262.
- [3] B. Wang, Q. Wang, H. Zhang, Z. Wang, W. Shen, S. Lee, H. Zhou, J. Tang, *Journal of Materials Chemistry A* **2025**, *13*, 35329-35341.
- [4] T. Chen, Y. Bai, X. Ji, W. Feng, T. Duan, X. Jiang, Y.-q.-q. Yi, J. Yu, G. Lu, X. Wan, B. Kan, Y. Chen, *Nano Energy* **2024**, *125*, 109604.
- [5] J. Xu, C. Xiao, Z. Zhang, J. Zhang, B. Wang, C. R. McNeill, W. Li, *Small* **2024**, *20*, 2405573.
- [6] K. Shi, H. Liu, S. Qin, Q. Zhao, X. Mou, J. Liang, J. Yao, C. Zhu, L. Zhong, J. Guo, J. Zhang, Y. Wu, Z.-G. Zhang, B. Qiu, Y. Li, *Angewandte Chemie International Edition* **2025**, *64*, e202514004.
- [7] H. Liu, H. Bai, Y. Zhou, P. Li, W. Su, C. Liu, X. Liao, B. Song, X. Li, Z. Bi, C. Zhao, H. Liu, G. Lu, H. Du, L. Jiang, Y. Liu, R. Ma, W. Ma, Q. Fan, *Materials Science and Engineering: R: Reports* **2025**, *162*, 100879.
- [8] C. Han, B. Cheng, Q. Guo, Z. Fu, J. Qiao, S. Cheng, Y. Huo, X. Xia, H. Wang, Y. Fu, X. Guo, X. Lu, X. Hao, Y. Li, M. Zhang, *Advanced Functional Materials* **2025**, *35*, 2416381.
- [9] L. Cao, H. Zhang, J. Du, Z. He, X. Du, H. Lin, C. Zheng, G. Yang, X. Li, S. Tao, *Journal of Energy Chemistry* **2025**, *103*, 19-26.
- [10] W. Su, X. Zhou, Q. Wu, Y. Wu, H. Qin, Z. Liang, H. Li, H. Bai, J. Guo, L. Jiang, Y. Liu, R. Ma, Y. Li, W. Zhu, Q. Fan, *Advanced Functional Materials* **2025**, *35*, 2415090.
- [11] T. Zhou, W. Jin, Y. Li, X. Xu, Y. Duan, R. Li, L. Yu, Q. Peng, *Advanced Science* **2024**, *11*, 2401405.
- [12] J. Zhou, C. Guo, L. Wang, C. Chen, Z. Gan, Y. Sun, C. Liu, J. Zhou, Z. Chen, D. Gao, W. Xia, D. Liu, T. Wang, W. Li, *Nano Energy* **2024**, *129*, 109988.
- [13] Y. Xu, X. He, Y. Tao, X. Ye, H. Chen, C.-Z. Li, *Journal of Energy Chemistry* **2025**, *103*, 458-464.
- [14] D. Wu, J. Peng, Y. Zhong, H. Guo, J. Zhou, L. Ye, J. Zhang, K. Han, H. Liu, X. Lu, M. Huang, B. Zhao, *Chemical Engineering Journal* **2025**, *524*, 168963.
- [15] B. Li, H. Xia, R. Ma, Y. Zhang, T. Zhu, Y. Liu, S. Chu, M. Zhu, X. Song, H. Tan, W. Zhu, *Chemical Engineering Journal* **2025**, *512*, 162655.
- [16] J. Yu, F. Wang, Y. Hao, P. Zhang, H. Bin, W. Zhu, H. Tan, *Small* **2025**, *n/a*, e10121.
- [17] R. Hao, H. Xia, X. Wang, H. Wei, J. Huang, F. Wang, Y. Zhang, H. Tan, M. Zhu, X. Song, Q. Fan, W. Zhu, *Chemical Engineering Journal* **2024**, *488*, 151067.
- [18] J. Song, C. Li, H. Ma, B. Han, Q. Wang, X. Wang, D. Wei, L. Bu, R. Yang, H. Yan, Y. Sun, *Advanced Materials* **2024**, *36*, 2406922.
- [19] P. Zhang, N. Gao, B. Du, Z. Xu, S. Wu, K. Zhu, X. Ma, H. Bin, Y. Li, *Angewandte Chemie International Edition* **2025**, *64*, e202424430.
- [20] Y. Xiao, X. Lu, *Mater Today Nano* **2019**, *5*, 100030.
- [21] Z. Wang, W. Wei, L. Zeng, T. Liu, X. Yuan, J. Zhou, B. Yin, J. Li, Z. Xie, F. Huang, Y. Cao, C. Duan, *Chemistry of Materials* **2023**, *35*, 6932-6942.
- [22] Q. Wei, S. Liang, W. Liu, Y. Hu, B. Qiu, J. Ren, J. Yuan, F. Huang, Y. Zou, Y. Li, *ACS*

- Energy Letters* **2022**, *7*, 2373-2381.
- [23] X. Xu, Q. Wei, J. Song, J. Jing, Y. Chen, F. Huang, X. Lu, Y. Zhou, J. Yuan, Y. Zou, *Journal of Materials Chemistry A* **2022**, *10*, 24717-24725.
- [24] S. Zhu, C. Shi, Q. Wei, C. Zhu, J. Ren, J. Li, L. Meng, Y. Li, J. Yuan, Y. Zou, *Chinese Journal of Chemistry* **2023**, *41*, 1815-1822.
- [25] Q. Wei, Y. Li, W. Chen, Q. Shi, S. Zhu, W. Yan, Y. Zou, *Journal of Materials Chemistry A* **2024**, *12*, 30558-30566.
- [26] B. Zhou, S. Liang, W. Chen, B. Fan, Q. Wei, Q. Shi, J. Yuan, Y. Zou, *Solar RRL* **2024**, *8*, 2400356.
- [27] D. Li, Y. Xu, W. Zhao, G. Cui, G. Li, B. Tang, *Solar RRL* **2023**, *7*, 2300413.
- [28] R. Ming, J. Gao, W. Gao, W. Ning, Z. Luo, F. Zhang, C. Yang, *Dyes and Pigments* **2021**, *185*, 108970.
- [29] W. Wei, X. Yuan, J. Zhong, Z. Wang, X. Zhou, F. Zhao, D. Feng, Y. Zhang, W. Chen, M. Yang, W. Zhang, Z. Ma, Z. Tang, X. Lu, F. Huang, Y. Cao, C. Duan, *Energy & Environmental Science* **2024**, *17*, 6627-6639.
- [30] W. Liu, H. Zhang, S. Liang, T. Wang, S. He, Y. Hu, R. Zhang, H. Ning, J. Ren, A. Bakulin, F. Gao, J. Yuan, Y. Zou, *Angewandte Chemie International Edition* **2023**, *62*, e202311645.
- [31] J. Song, F. Cai, C. Zhu, H. Chen, Q. Wei, D. Li, C. Zhang, R. Zhang, J. Yuan, H. Peng, S. K. So, Y. Zou, *Solar RRL* **2021**, *5*, 2100281.